Bulletin of the Seismological Society of America, Vol. 84, No. 3, pp. 725–734, June 1994

# Local Observations of the Onset of a Large Earthquake: 28 June 1992 Landers, California

by Rachel Abercrombie and Jim Mori

**Abstract** The Landers earthquake ($M_w$ 7.3) of 28 June 1992 had a very emergent onset. The first large amplitude arrivals are delayed by about 3 sec with respect to the origin time, and are preceded by smaller-scale slip. Other large earthquakes have been observed to have similar emergent onsets, but the Landers event is one of the first to be well recorded on nearby stations. We used these recordings to investigate the spatial relationship between the hypocenter and the onset of the large energy release, and to determine the slip function of the 3-sec nucleation process. Relative location of the onset of the large energy release with respect to the initial hypocenter indicates its source was between 1 and 4 km north of the hypocenter and delayed by approximately 2.5 sec. Three-station array analysis of the *P* wave shows that the large amplitude onset arrives with a faster apparent velocity compared to the first arrivals, indicating that the large amplitude source was several kilometers deeper than the initial onset. An $M_L$ 2.8 foreshock, located close to the hypocenter, was used as an empirical Green's function to correct for path and site effects from the first 3 sec of the mainshock seismogram. The resultant deconvolution produced a slip function that showed two subevents preceding the main energy release, an $M_w$ 4.4 followed by an $M_w$ 5.6. These subevents do not appear anomalous in comparison to simple moderate-sized earthquakes, suggesting that they were normal events which just triggered or grew into a much larger earthquake. If small and moderate-sized earthquakes commonly "detonate" much larger events, this implies that the dynamic stresses during earthquake rupture are at least as important as long-term static stresses in causing earthquakes, and the prospects of reliable earthquake prediction from premonitory phenomena are not improved.

## Introduction

One interesting aspect of the 28 June 1992 Landers earthquake ($M_w$ 7.3) is its emergent onset. Seismograms of the event recorded at local and regional stations all show several seconds of small but increasing amplitude arrivals followed by the onset of the main energy release, approximately 3 sec after the origin time. This observation is confirmed by the triggering of almost all of the local California Division of Mines and Geology (CDMG) strong-motion stations 3 sec or more after the expected *P*-wave arrival times from the mainshock origin time. Large arrivals at broadband teleseismic stations are also approximately 3 sec later than expected from the origin time from the local short-period network (Wald and Heaton, 1994). A number of authors have modeled the slip of the Landers rupture, and have experienced similar problems with timing. The model slip arrives before the actual slip in the observed seismograms, so a delay of 2.5 to 3 sec was introduced between the origin time (from the short-period network) and the beginning of the large rupture (Campillo and Archuleta, 1993; Cohee and Beroza, 1994; Dreger, 1994; Wald and Heaton, 1994). The models from all these authors fit the observed seismograms well, indicating that relatively little slip occurred in the first few seconds. At a typical rupture velocity of 2.7 km/sec (Wald and Heaton, 1994), a 2.5- to 3-sec delay implies that the origin of the large energy release could be over 8 km from the hypocenter of the earthquake; however, for their models to be correct, the rupture could not have propagated far in those first few seconds.

Determining what occurred during the first 3 sec of the Landers earthquake is important for improving the accuracy of models of the later, larger rupture, and also will provide us with much-needed information about how large earthquakes nucleate and grow. Theoretical and experimental models of earthquake nucleation suggest

that preparation zones may have dimensions of anything from millimeters to kilometers (e.g., Dieterich 1986; Ohnaka, 1993). Clearly, the scale of the preparation zone and the style of earthquake nucleation control any possibility of future earthquake prediction. Perhaps the simplest viewpoint is to consider whether it is what starts the earthquake or what stops it that determines the final rupture size. Is the size of the preparation zone proportional to the final size, or is any small earthquake (presumably with some sort of very small "nucleation zone") capable of growing into or triggering a much larger rupture if nothing stops it (for example, as in the numerical models of Bak and Tang, 1989)? In the latter case, the nucleation zones may be identical for a small earthquake and for a much larger, damaging one.

The Landers earthquake is not the first to show such an emergent onset. Previous studies (e.g., Abercrombie, 1991; Choy and Dewey, 1988; Haessler *et al.*, 1992; Wald *et al.*, 1991) have seen small initial subevents, around 1% of the total earthquake moment, preceding the main event by one to tens of seconds. Small initial slip may therefore not be uncommon, but it is difficult to detect. The local short-period instruments tend to record the onset but soon clip on the subsequent larger arrivals. Triggered strong-motion instruments often miss the initial onset, and teleseismic data rarely have the sensitivity to resolve it. The Landers earthquake, however, was well recorded by seven local stations, which were sensitive enough to see the onset clearly and with wide enough dynamic range not to clip on the larger, later arrivals from the main energy release. In this article, we first investigate the spatial relationship between the hypocenter of the Landers earthquake and the onset of the main energy release. We then analyze in detail the first 3 sec of the Landers earthquake for information concerning its nucleation and early growth.

Table 1
The Seven Stations Used in the Relative Location of the Onset of the Large Energy Release*

| Station Name | Station Code | Distance (km) | Time Delay (sec) |
|---|---|---|---|
| Morongo Valley | MVB | 21.0 | 3.05–3.65 |
| East Wide Canyon | EWC | 29.1 | 3.5 |
| Fire House | FHS | 31.7 | 3.4–3.6 |
| Piñon Flats | PFO | 64.9 | 3.23–3.48 |
| Cajon Pass Borehole | CJP | 96.6 | 2.77–3.17 |
| Goldstone Lake | GSC | 127.6 | 2.24–3.10 |
| Pasadena | PAS | 159.6 | 3.25–3.65 |

*The distance is that between the Landers hypocenter and receiver, and the time delay is that between the first arrival and that of the first large amplitude waves.

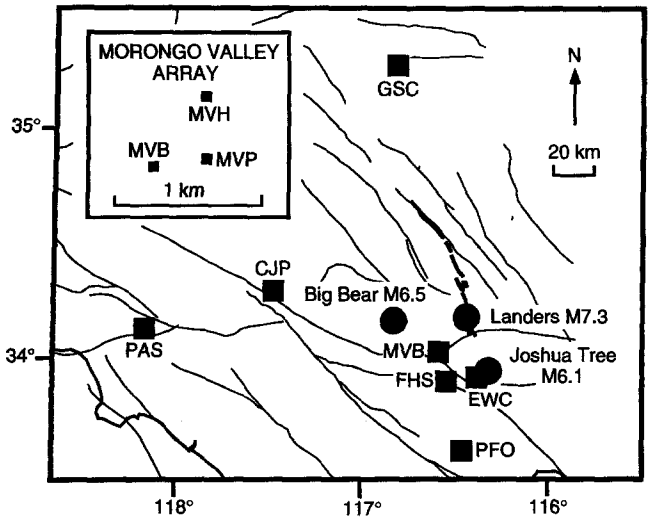


Figure 1. Fault map showing the location of the three principal earthquakes in the Landers sequence, April to June 1992, and the seven stations used in this study. The Landers surface rupture is shown in bold. *Inset* shows three stations of the Morongo Valley array used for the slowness analysis.

## Location of the Large Energy Onset

Stations at seven local sites recorded both the initial onset and the arrival of the first large amplitude waves of the Landers mainshock clearly enough to use relative arrival times to locate the onset of the large energy. These stations are listed in Table 1 and shown in Figure 1. Two are GEOS (Borcherdt *et al.*, 1985) portable stations, deployed to record aftershocks of the Joshua Tree earthquake (MVB, FHS). The station EWC is a strong-motion station of the Southern California Seismic Network. Three stations of the high dynamic range TERRAscope network (Kanamori *et al.*, 1991) recorded the onset clearly (PFO, GSC, PAS). The seventh station is the 2.5-km-deep borehole instrument near Cajon Pass (CJP, Abercrombie and Leary, 1993).

The onset of the Landers mainshock recorded at the extremely low-noise borehole station (Fig. 2) and high-gain, short-period stations within 20 km of the epicenter, confirms that the origin time determined by the Southern California Seismic Network is correct, and that no smaller event preceded it. These stations would not have detected a long-period type of precursory event, but strain data from Piñon Flat indicate that there were no such signals (Wyatt *et al.*, 1994). The arrival of the large amplitude waves was most easily seen on displacement waveforms obtained from twice integrating the acceleration records (Fig. 3). The initial onset could be chosen to within about 0.05 sec on the high-gain channels, but identifying the beginning of the large energy release was less clear, so a range of possible times was selected. The range of time delays at each station was subdivided into 0.1-sec intervals, and each was added to the calculated travel time from the Landers hypocenter to the station (Table 1). The depth of the initial hypocenter is poorly

known because of the lack of identifiable shear wave arrivals. Hauksson *et al.* (1993) constrain the depth to be 3 to 6 km, and 4.5 km is used here. Shear wave arrivals from the large amplitude onset were identified on the transverse components at MVB and EWC and included to help constrain the location. The program HYPOINVERSE (Klein, 1985) with a local velocity model (Table 2) determined by Eberhart-Phillips (personal comm.) was used to locate every possible combination of travel times at the seven stations (over 800).

The resulting range of possible locations for the onset of the main energy release is shown in Figure 4. The lack of stations to the east results in poor east–west resolution in the locations, causing the "cloud" of locations to be poorly aligned with the fault. The average delay between the origin time and the onset of the main energy release is 2.5 sec, and in this time, the rupture moved between 1 and 4 km north from the hypocenter. There is no indication of rupture to the south. This is consistent with the later northward propagation of the large mainshock rupture (e.g., Kanamori *et al.*, 1992; Campillo and Archuleta, 1993; Cohee and Beroza, 1994; Dreger, 1994; Wald and Heaton, 1994). There is little constraint on the depth in this location of the onset of the large amplitude; however, we will present more information on the depth in the next section.

## Small Aperture Array Observations of the Onset

The station MVB was part of a small array of four sites spaced at distances of a few hundred meters (Hough *et al.*, 1993), of which three stations (Fig. 1) recorded

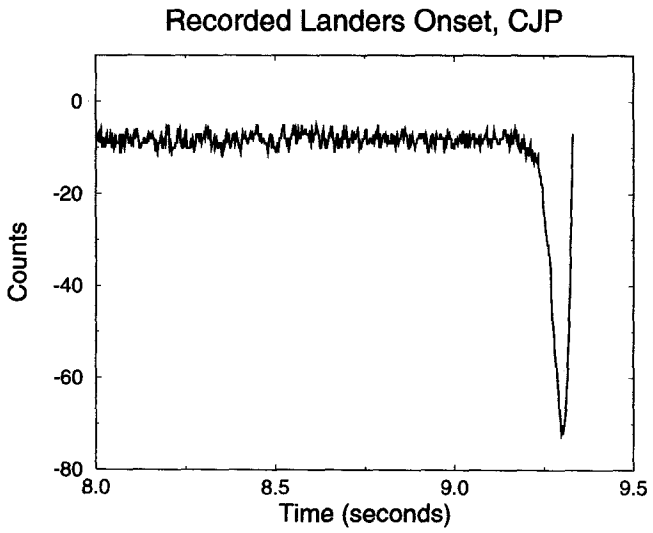


Figure 2. The first onset (recorded velocity) at the deep borehole station at Cajon Pass. The first small subevent which triggered the short-period network was clearly not preceded by any detectable smaller slip.

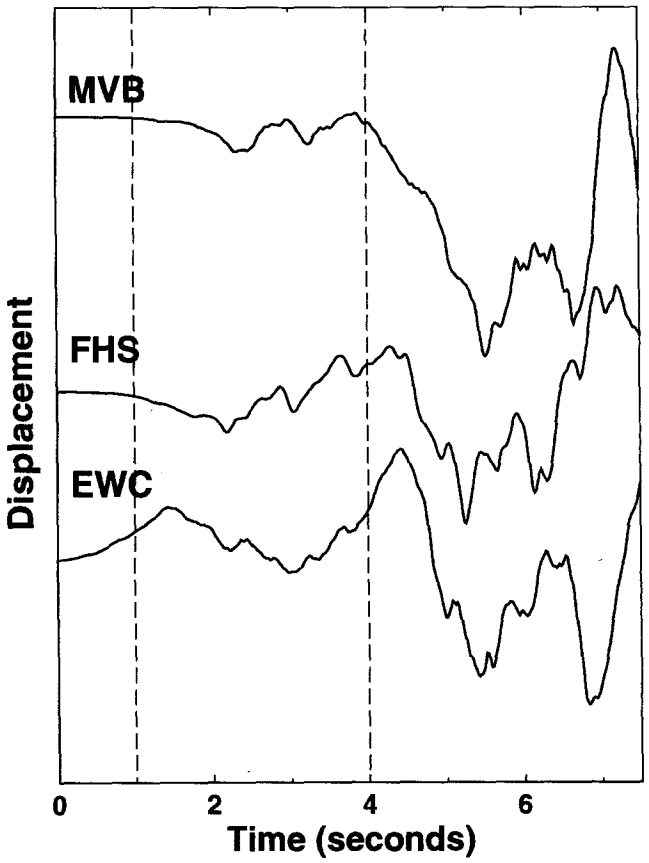


Figure 3. The vertical displacement records (integrated from acceleration) of the onset of the Landers mainshock from the three nearest stations. They are aligned by their first arrivals, the onset of the small slip (first dotted line), at 1.0 sec in the figure. The onset of the large slip is delayed by approximately 3 sec at all stations, and is roughly indicated by the second dotted line, 3 sec after the first.

Table 2
Velocity Structure Used to Locate the Earthquakes

| *P* Velocity (km/sec) | Depth (km) |
|---|---|
| 4.69 | 0.0 |
| 5.61 | 3.0 |
| 5.98 | 5.0 |
| 6.05 | 7.0 |
| 6.12 | 9.0 |
| 6.22 | 11.0 |
| 6.37 | 14.0 |
| 6.56 | 18.0 |
| 6.76 | 22.0 |
| 7.05 | 26.0 |
| 7.70 | 32.0 |

the initial onset on vertical velocity components. These records were used to estimate the azimuth of approach and apparent velocity for the incoming $P$ wave using a moving-window slowness analysis (Frankel *et al.*, 1991). This type of analysis has been used to map rupture propagation in strong-motion records (Spudich and Cranswick, 1984), identify approaching waves in two dimensions from Loma Prieta aftershocks (Frankel *et al.*, 1991) and a large Landers aftershock (Hough *et al.*, 1993, using these same data), and measure wavefronts in three dimensions at Garni, Armenia (Mori *et al.*, 1994).

For an incident plane wave, the arrival time ($t_i$) at station $i$ can be written as

$$t_i = S_x x_i + S_y y_i.$$

The terms $S_x$ and $S_y$ are the horizontal components of slowness, and $x_i$ and $y_i$ are the spatial coordinates of the station. For each time window, we tested all values of $S_x$ and $S_y$ from 0 to 0.3 sec/km at intervals of 0.005 sec. The best-fitting slowness was determined by cross-correlating each pair of seismograms (three pairs for the three stations), averaging the values together, and choosing the slowness with the highest average correlation. The correlation function ($h$) we used to correlate two time series **f** and **g** was as follows:

$$h = \frac{\Sigma f_i g_i}{\sqrt{\Sigma f_i^2 \, \Sigma g_i^2}}.$$

We used windows that were 0.5-sec long with a 10% cosine taper on the ends, and successive windows were offset by 0.05 sec. Slowness estimates were made for the first 3.0 sec of the velocity records before the amplitudes become clipped. We were not able to use the strong-motion accelerometer records from the array because only two of the stations recorded the event on the vertical acceleration channel.

From the slowness estimate, the incoming azimuth of the wave is

$$\phi = \arctan (S_x/S_y),$$

and the apparent velocity is

$$V_a = 1/(S_x^2 + S_y^2)^{1/2}.$$

The absolute timing at the stations was not accurate enough for this analysis, so we fixed the time window of the first arrival to have an apparent velocity of 5.6 km/sec from the azimuth of the initial location. The initial velocity assumes the hypocenter was at a depth of 4.5 km within a crustal layer that has $P$-wave velocity of 5.6 km/sec.

The results for the incoming azimuth and apparent velocity for the various time windows are shown in Figures 5a and 5b, respectively. The larger circles are for values that had an average correlation of greater than 0.8, reflecting better-correlated arrivals and, thus, are considered to be more reliable. There are three groups of well-correlated arrivals in Figure 5: (1) the initial onset which was fixed to arrive from the hypocenter; (2) an arrival about half a second later with the same azimuth and velocity; and (3) the beginning of the large amplitude onset about 2.5 sec into the event that is arriving from more northerly azimuths and with higher apparent velocity. These three groups of arrivals correspond to the first two subevents and the onset of the large amplitude arrival, which are identified in the following section.

The azimuth and the apparent velocity stay relatively constant over the first 2.5 sec of the event. During this time, the well-correlated arrivals vary in azimuth by ±3 deg from the initial onset, which corresponds to distances of ±1.5 km along the fault. The apparent velocities vary by about ±0.3 km/sec, with the second group of arrivals slightly slower than the initial arrival, possibly indicating a slightly shallower source. For time windows near the large amplitude onset, the azimuths are scattered but show a swing toward the north with values averaging 5 deg north of the initial arrival. This corresponds to a distance of 2.8 km along the fault north of the initial epicenter and is consistent with the location of the large amplitude onset obtained in the previous section. The most significant change observed in this analysis is the increase in apparent velocity at about 2.5 sec. The velocities for the well-correlated arrivals in this third group increase to values of 5.9 to 6.7 km/sec with an average of 6.2 km/sec. The higher apparent velocities

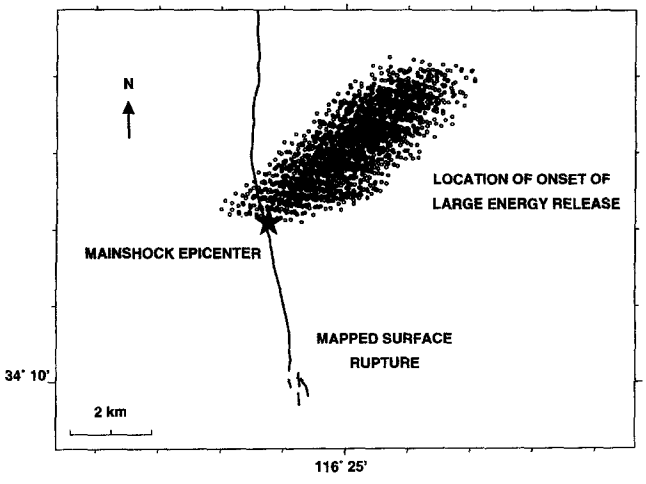


Figure 4. The map view of the relative location results showing the possible range of locations of the onset of the large energy release with respect to the epicenter (star). The mapped surface rupture is also included.

can be interpreted as energy that is arriving from a deeper source. Assuming the velocity model in Table 2, the source depth for the large amplitude onset corresponding to the observed apparent velocity of 6.2 km/sec is 9 to 11 km. Another explanation is that the higher-velocity arrivals are from a high-angle reflection from a crustal layer. However, this is unlikely because the amplitude of the reflection would have to be very large to dominate over the growing amplitude of the direct *P* wave. Also, there is no evidence for such a phase in the small earthquake used as an empirical Green's function, shown in the following section.

We tried other values for the apparent velocity of the initial arrival and found that the pattern shown by the successive time windows did not change. Even if we used an incorrect value for the initial velocity (initial depth of the hypocenter), the conclusion is still valid that the energy beginning 2.5 sec into the event is arriving from greater depth.

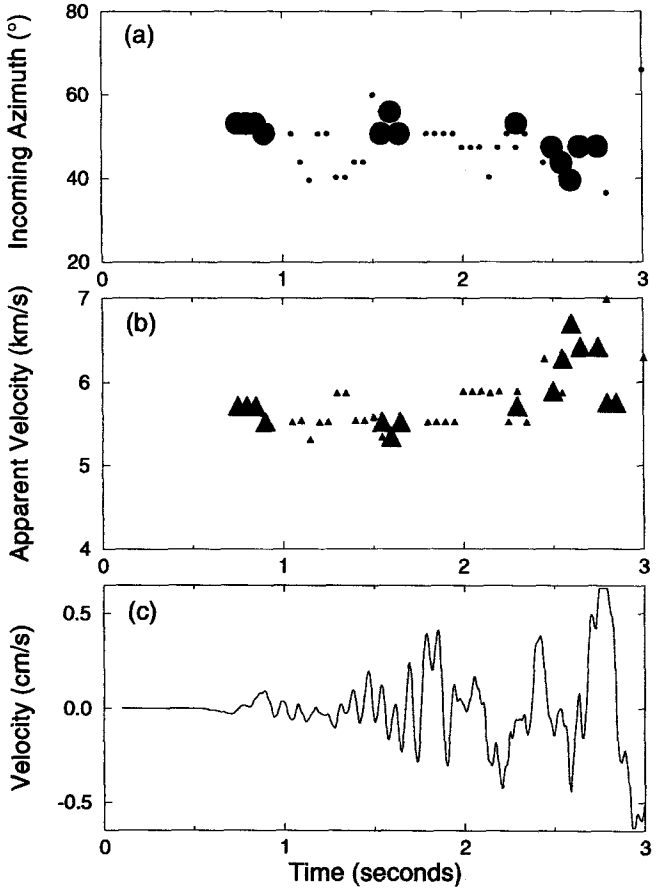


Figure 5. Incoming azimuth (a) and apparent velocity (b) estimates for 0.5-sec time windows of the first 2.5 sec of the *P* wave recorded on the Morongo Valley array (onset time is at 0.5 sec). Large/small symbols are for arrivals that had average cross-correlations larger/smaller than 0.8. The seismogram (c) is an example of one of the three seismograms used in the analysis.

## Slip History of the First Three Seconds

In order to elucidate further the nucleation and early growth of the Landers mainshock, we used the empirical Green's function technique to deconvolve out the slip function of the first few seconds. Many recent studies (e.g., Mueller, 1985; Frankel *et al.*, 1986) have used this technique with success to remove site and path effects from short-period seismograms. A small earthquake, co-located with the event of interest and small enough to be considered a point source, is selected. The form of the seismograms of this small (Green's function) event can thus all be attributed to path and site effects. Deconvolving the seismograms of this event from those of the earthquake of interest at the same stations should therefore remove all these effects, revealing the source time function of the larger event.

We used the Morongo Valley station MVB to obtain the slip function of the first 3 sec of the Landers mainshock. Other stations were located at *P*-wave nodes or at regional distances where the wave trains were emergent and not suitable for the deconvolution. The seismicity catalog was searched for small events ($M_L$ 2.0 to 3.5) close to mainshock hypocenter, and one of the larger foreshocks ($M_L$ 2.8), with a similar focal mechanism to the mainshock, was selected as the Green's function event (Table 3). Since the mainshock was recorded on scale on the strong-motion accelerometer and the Green's function event on the higher-gain velocity transducer, the relevant instrument responses were removed from both records. The records were converted to velocity and bandpass-filtered between 0.2 and 20 Hz. A 3-sec length of the Green's function seismogram, including 1 sec of pre-event noise, and a 15-sec length of the mainshock seismogram, including 1.4 sec pre-event noise, were used for the deconvolution. The deconvolution was performed in the time domain using a linear least-squares filter similar to the analysis of Hartzell and Heaton (1985) to find the time series **x** that solves

$$\mathbf{Ax} = \mathbf{B},$$

where **A** is the matrix that describes the convolution with the Green's function event $g(t)$,

$$A_{ij} = g(t_{i-j}),$$

and **B** is the mainshock time series. No smoothing or positivity constraints were imposed on the inversion.

The time series $x(t)$ which represents the displacement source time function is shown in Figure 6. This slip function reveals a small initial pulse with a duration of about 0.5 sec, a second, larger, and more complicated pulse beginning at about 1.0 sec with a duration of 2.0 sec, and then the start of the large amplitude onset beginning at 3 sec (i.e., 2.5 sec after the initial onset). We

Table 3
Hypocentral Parameters of the Earthquakes Considered in This Study (Time in Hours, Minutes, and Seconds)

| Event | Date | Time (UTC) | $M$ | Latitude | Longitude | Depth (km) |
|---|---|---|---|---|---|---|
| Foreshock | 28 June 1992 | 10:52:06.59 | 2.8 | 34°11.80′ | −116°26.35′ | 3.0 |
| Mainshock | 28 June 1992 | 11:57:34.12 | 7.3 | 34°12.07′ | −116°26.13′ | 4.5 |
| Aftershock | 29 June 1992 | 03:01:56.38 | 4.4 | 34°14.32′ | −116°26.58′ | 7.5 |

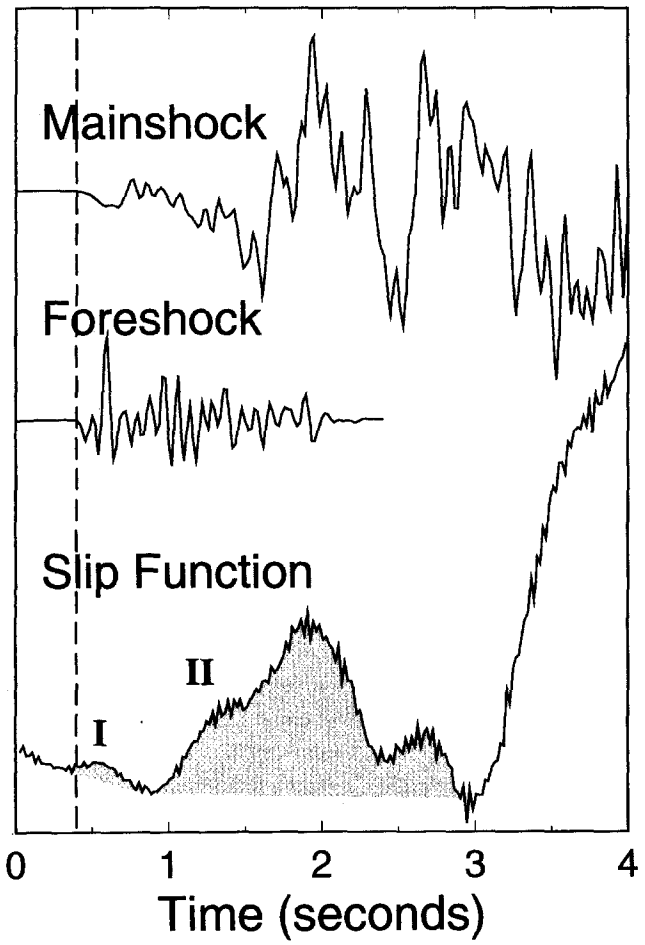


Figure 6. Mainshock velocity record (*top*), $M_L$ 2.8 foreshock used as an empirical Green's function (*middle*), both recorded at MVB, and resultant deconvolution showing the displacement source time function (*bottom*). The first arrivals of the mainshock and foreshock are aligned with the resulting slip function. The dotted line shows the time of the first arrival. The two subevents I and II and the onset of the large energy release about 2.6 sec after the start of I can clearly be seen.

interpret the first two pulses as early subevents of the Landers mainshock, and calculate their moments from the pulse areas [shown by the shaded areas ($A$) in Fig. 6] using the expression from Brune (1970),

$$M_0 = \frac{4\pi\rho R\alpha^3}{U_{\phi\theta}} A,$$

where $R$ is the hypocentral distance, $\rho$ is the density (2800 kg/m$^3$), $\alpha$ is the $P$-wave velocity (5.6 km/sec), and $U_{\phi\theta}$ is the radiation pattern correction which includes the free surface effect (0.73 at MVB). The resulting source parameters, including the moment magnitudes ($M_w$, Hanks and Kanamori, 1979) are shown in Table 4.

The first subevent (I) has a moment of $4.6 \times 10^{15}$ N-m ($M_w$ 4.4), and the second subevent (II), which begins half a second later, has a moment of $2.6 \times 10^{17}$ N-m ($M_w$ 5.6). The sizes of these subevents are consistent with the triggering of the CDMG strong-motion instruments. The majority were not triggered until after the onset of the main energy release (>3 sec after the initial $P$-wave arrival). Nine out of the twenty-five nearest stations (12- to 85-km hypocentral distance) triggered at delays of 0.8 to 1.7 sec with respect to the initial $P$-wave arrival and appeared to have been triggered by the second subevent.

The estimates of source size and stress drop are model dependent and more difficult to make, particularly from only one station. A fault radius ($r$) assuming a circular fault that ruptures according to the model of Boatwright (1980) can be calculated using

$$r = \frac{t_{1/2}V}{\left[1 - \frac{V \sin\theta}{\alpha}\right]},$$

where $t_{1/2}$ is the rise time of the far-field pulse, $V$ is the rupture velocity (2.7 km/sec, Wald and Heaton, 1994), and $\theta$ is the take-off angle measured from the fault normal. This formulation gives fault radii of 1.1 and 4.4 km for subevents I and II, respectively. If the subevents broke in a more unilateral fashion, the ruptures would have lengths of 1.4 and 5.4 km for subevents I and II, respectively. With these considerations, we estimate the dimension of subevent I to be 1 to 3 km and subevent II to be 5 to 9 km.

A static stress drop can be estimated using

$$\Delta\sigma = c\frac{M_0}{d^3},$$

where c is a constant near 1 and $d$ is a fault dimension (Kanamori and Anderson, 1975). For a circular fault, c

Table 4
Source Parameters of the Two Early Subevents of the Landers Mainshock Determined from the Slip Function at MVB

| Event | Moment (N-m) | $M_w$ | Duration (sec) | Dimension (km) | Stress Drop (bars) | Arrival Time (sec) |
|---|---|---|---|---|---|---|
| I | $4.6 \times 10^{15}$ | 4.4 | 0.5 | 1–3 | 11–15 | 0.0 |
| II | $2.6 \times 10^{17}$ | 5.6 | 2.0 | 5–9 | 11–13 | 0.5 |

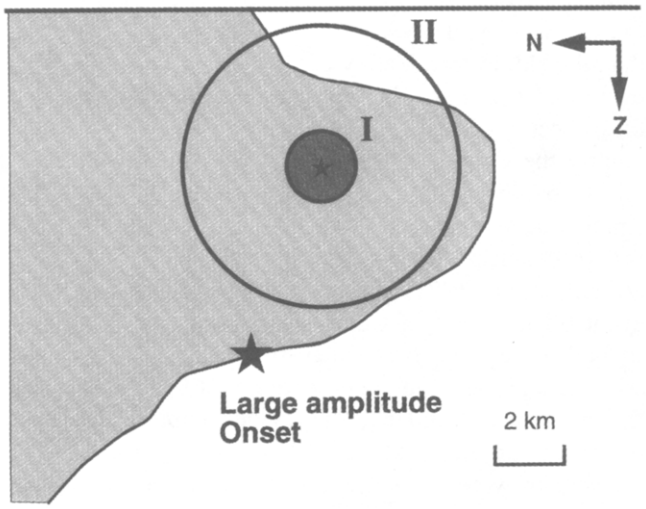


Figure 7. Cartoon-style vertical cross section (no vertical exaggeration) of the first 3 sec of the Landers rupture showing the locations and sizes of the two early subevents (I and II) and the onset of the large amplitudes. Shaded portion is the area of slip for the Landers earthquake derived by Wald and Heaton (1994).

$= 7/16$, and $d$ is the fault radius. For a rectangular strike-slip fault, $c = 2/\pi$, and $d^3$ is the $(\text{width})^2 * (\text{length})$. Assuming a circular rupture, the static stress drops are 15 and 13 bars for subevents I and II, respectively. For a unilateral rupture with the fault width equal to the fault length, the stress drop of both subevents I and II was 11 bars.

## Discussion

The preceding analyses of the first 3 sec of the Landers earthquake show that it began with an $M_w$ 4.4 subevent, followed about 0.5 sec later by an $M_w$ 5.6 subevent and then by the main rupture, approximately 2.5 sec after the initial onset. The hypocenter of the main rupture is less than 4 km to the north of the $M_w$ 4.4 event, at a depth several kilometers deeper than the first two subevents. The constraints on the location and size of the two initial subevents are used to show their spatial relationship to the onset of the large amplitudes (Fig. 6). The location and depth of the first subevent and the large onset are relatively well constrained, but little is known about subevent II, except that the array analysis indicates that it is located close to subevent I at about the same depth or slightly shallower. The sequence sketched in Figure 7 shows subevents I ($M_w$ 4.4) and II ($M_w$ 5.6) occurring at similar locations at relatively shallow depth. The large energy release initiates 2.5 sec later, a few kilometers to the north and at greater depth, near the base of the seismogenic zone. The maximum depth of aftershocks in the hypocentral area is about 14 km (Hauksson *et al.*, 1993), and many earthquakes that rupture the entire brittle crust nucleate near its base (Sibson, 1983). This onset of the large energy release may have occurred near the edge of subevent II. The shaded area in Figure 7 shows the area of slip for the Landers earthquake derived from strong-motion records by Wald and Heaton (1994) and indicates that once the large energy release began, the earthquake ruptured upward and to the north, rerupturing the areas that slipped during subevents I and II. The onset of the large energy release at the edge of subevent II is similar to the Joshua Tree sequence, in which the mainshock initiated at the edge of the foreshock rupture area (Mori, 1994).

The onset of the Loma Prieta earthquake was also emergent, with a 2.5-sec delay between the origin time and the onset of the main energy release (Wald *et al.*, 1991). Detailed analysis of the first few seconds of this earthquake is problematic because of the small amount of unclipped local data. There is some evidence, however, that the earthquake began with an $M$ 5.8 subevent, and that this early rupture was very smooth, radiating relatively little high-frequency energy (Ellsworth, 1992). We could find no such apparent lack of high frequencies radiated by the early subevents of the Landers earthquake, nor any evidence for anomalous long-period energy. The empirical Green's function analysis was carried out between 0.2 and 20 Hz. It is possible that the foreshock recording on the velocity transducer may be contaminated with low-frequency noise, but it was not obvious in the seismograms (Fig. 6), and it would be fortuitous if that noise exactly matched any long-period energy in the mainshock record so as to cancel it out completely in the deconvolution. In order to check our results, we compared the onset of the Landers mainshock with that of a co-located $M_L$ 4.4 aftershock recorded on the strong-motion accelerometer (Table 3, Fig. 8). The two records look similar in the first half-second,

before the arrival of subevent II in the mainshock record. There may be a little more high-frequency energy in the aftershock record, but it could just be a higher stress drop earthquake. The stress drops estimated for subevents I and II of the mainshock are at the lower end of the normal range for tectonic earthquakes (10 to 1000 bars, Abercrombie and Leary, 1993). It is possible that some anomalous longer-period energy (<0.2 Hz) was radiated by the Landers onset, but using the available data, we could find no evidence for its existence. This conclusion is supported by the teleseismic observations. Prominent arrivals on teleseismic broadband and long-period records are delayed by about 3 sec with respect to the travel time from the origin time (Wald and Heaton, 1994), while short-period arrivals with amplitudes consistent with an $M$ 4 event come in at the expected arrival time. The lack of observed anomalous long-period energy argues against the early slip in the Landers earthquake being slow or distinguishable from ordinary earthquakes. One other difference between the onsets of the Landers and Loma Prieta earthquakes is their depth. The early subevents to Landers were about 5-km deep, compared to the 18-km depth of the hypocenter at Loma Prieta (Wald *et al.*, 1991), and this difference may be related to their apparent difference in character.

If the Landers earthquake was triggered by an ordinary $M_w$ 4.4 shallow earthquake, then a number of interesting questions require consideration. For example, why did the mainshock not take place 13 yr earlier following the Homestead Valley ($M$ 5.2) earthquake (Hutton *et al.*, 1980)? Extra strain built up in the last 13 yr is probably insignificant when the recurrence time is several thousand years (Sieh *et al.*, 1993). Also, why did the Joshua Tree earthquake ($M_w$ 6.1), that occurred 2 months earlier, not continue north if the faults which slipped in the Landers earthquake were so near to failure? Without more detailed knowledge about what starts and stops earthquake rupture, and also about the local stress conditions in the crust in the area of Landers and Joshua Tree, these are difficult questions to answer. It would appear that a moderate-sized earthquake will grow into, or trigger, a much larger event only given a very limited set of conditions. The $M_w$ 4.4 first subevent of the Landers mainshock may have been more successful than the Homestead Valley earthquake in causing a large event because it was better positioned with respect to a local asperity or change in material properties which could control the growth of the rupture.

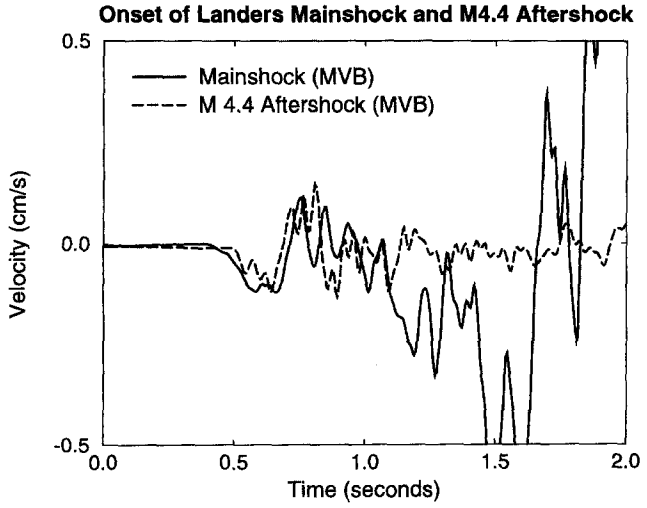


Figure 8. The beginning of the Landers mainshock (solid line) and a $M_L$ 4.4 aftershock (dashed line) velocity seismograms recorded at MVB. Both records were recorded on the strong-motion accelerometer, integrated and filtered between 0.2 and 20 Hz.

Two other examples of earthquakes in which two small subevents preceded the main rupture are the 1981 ($M_s$ 6.6) normal faulting event in the Gulf of Corinth (Abercrombie, 1991) and the 1985 ($M_s$ 7.8) subduction event off the coast of Chile, (Choy and Dewey, 1988). In both cases, the first subevent was smaller than the second, and their moments were about 0.01 and 1% of the mainshock, similar to the Landers rupture. It is also interesting to note that events preceding the Chilean earthquake were located updip of the deeper main rupture (Choy and Dewey, 1988).

There is evidence for small initial subevents to a number of larger earthquakes from strike slip, normal faulting, and subduction regimes. The presence of these small preliminary events raises a number of questions. For example, is it possible to identify which moderate-sized earthquakes will grow into (or trigger) much larger events? Another possibility is that moderate-sized earthquakes may actually be necessary to "detonate" large and great earthquakes, but often go undetected as they do not trigger strong-motion instruments and are difficult to see teleseismically because of their small size. If such triggering is not anomalous, then it would suggest that dynamic, co-seismic stresses could play a significant role in determining the extent of earthquake rupture, such as in the dynamic slip pulse model (Heaton, 1990). The entire slip function of the Landers earthquake (combining the results presented here with the later models from, for example, Wald and Heaton, 1994) is similar to those of the numerical "earthquakes" of Bak and Tang (1989). Brune (1979) considered the implications of large events commonly initiating as much smaller events, and showed that if this is the case, it will be difficult to predict large earthquakes from premonitory phenomena.

## Conclusions

Analysis of the first 3 sec of the Landers mainshock reveals that two subevents preceded the onset of the large energy release. The first ($M_w$ 4.4) was followed half a second later by a larger subevent ($M_w$ 5.6). Relative lo-

cation and array analysis of the onset of the large energy release constrain it to within 1 to 4 km north of the hypocenter and at depths several kilometers deeper than the initial subevents. The initiation of the main energy release appeared to have started on the edge of the second subevent and ruptured upward and to the north, rerupturing the area of the preliminary subevents.

The first subevent of the Landers earthquake appeared indistinguishable from a typical moderate-sized earthquake, and there are a number of other examples of small preliminary slip to large earthquakes in the literature. The initiation of large earthquakes by much smaller events may, therefore, not be uncommon, and this raises questions about the future possibility of reliable earthquake prediction.

## Acknowledgments

We are grateful to G. Glassmoyer and S. Hough for providing us with the Morongo Valley records and to D. Eberhart-Phillips for providing the local velocity structure. We thank D. Dreger, D. Wald, and B. Cohee for their preprints. Helpful comments on the manuscript were provided by T. Heaton, S. Hough, and two anonymous reviewers. REA is supported by a Southern California Earthquake Center (SCEC) Fellowship, and this is SCEC publication number 76.

## References

Abercrombie, R. E. (1991). Earthquake rupture dynamics and neotectonics in the Aegean region, *Ph.D. Thesis*, University of Reading, United Kingdom.

Abercrombie, R. E. and P. C. Leary (1993). Source parameters of small earthquakes recorded at 2.5 km depth, Cajon Pass, southern California: implications for earthquake scaling, *Geophys. Res. Lett.* **20**, 1511–1514.

Bak, P. and C. Tang (1989). Earthquakes as a self-organized critical phenomenon, *J. Geophys. Res.* **94**, 15635–15637.

Boatwright, J. (1980). A spectral theory for circular seismic sources: simple estimates of source dimension, dynamic stress drops, and radiated energy, *Bull. Seism. Soc. Am.* **70**, 1–28.

Borcherdt, R. D., J. B. Fletcher, E. G. Jensen, G. L. Maxwell, J. R. VanSchaak, R. E. Warrick, E. Cranswick, M. J. S. Johnston, and R. McClearn (1985). A general earthquake observation system (GEOS), *Bull. Seism. Soc. Am.* **75**, 1783–1826.

Brune, J. (1970). Tectonic stress and the spectra of seismic shear waves from earthquakes, *J. Geophys. Res.* **75**, 4997–5009.

Brune, J. (1979). Implications of earthquake triggering and rupture propagation for earthquake prediction based on premonitory phenomena, *J. Geophys. Res.* **84**, 2195–2198.

Campillo, M. and R. J. Archuleta (1993). A rupture model for the 28 June 1992 Landers, California earthquake, *Geophys. Res. Lett.* **20**, 647–650.

Choy, G. L. and J. W. Dewey (1988). Rupture process of an extended earthquake sequence: teleseismic analysis of the Chilean earthquake of March 3, 1985, *J. Geophys. Res.* **93**, 1103–1118.

Cohee, B. P. and G. C. Beroza (1994). An extended source model for the 1992 Landers mainshock, *Bull. Seism. Soc. Am.* (in press).

Dieterich, J. H. (1986). A model for the nucleation of earthquake slip, in *Earthquake Source Mechanics*, S. Das, J. Boatwright, and C. H. Scholz (Editors), Geophysical Monograph 37, Maurice Ewing Vol. 6, American Geophysical Union, Washington D.C., 37–47.

Dreger, D. (1994). Investigation of the rupture process of the June 28, 1992 Landers earthquake utilizing TERRAscope data, *Bull. Seism. Soc. Am.* **84**, no. 3, 713–724.

Ellsworth, W. L. (1992). Imaging fault rupture without inversion (abstract), *Seism. Res. Lett.* **63**, 73.

Frankel, A., S. Hough, P. Friberg, and R. Busby (1991). Observations of Loma Prieta Aftershocks from a dense array in Sunnyvale, California, *Bull. Seism. Soc. Am.* **81**, 1900–1922.

Frankel, A., J. Fletcher, F. Vernon, L. Haar, J. Berger, T. Hanks, and J. Brune (1986). Rupture characteristics and tomographic source imaging of ML ~ 3 earthquakes near Anza, southern California, *J. Geophys. Res.* **91**, 12633–12650.

Haessler, H., A. Deschamps, H. Dufumier, H. Fuenzalida, and A. Cisternas (1992). The rupture process of the Armenian earthquake from broad-band teleseismic body wave records, *Geophys. J. Int.* **109**, 151–161.

Hanks, T. C. and H. Kanamori (1979). A moment magnitude scale, *J. Geophys. Res.* **84**, 2348–2350.

Hartzell, S. H. and T. H. Heaton (1985). Teleseismic time functions for large shallow subduction zone earthquakes, *Bull. Seism. Soc. Am.* **75**, 965–1004.

Hauksson, E., L. M. Jones, K. Hutton, and D. Eberhart-Phillips (1993). The 1992 Landers earthquake sequence: seismological observations, *J. Geophys. Res.* **98**, 19835–19858.

Heaton, T. H. (1990). Evidence for and implications of self-healing pulses of slip in earthquake rupture, *Phys. Earth Planet. Interiors* **64**, 1–20.

Hough, S. E., J. Mori, E. Sembera, G. Glassmoyer, C. Mueller, and S. Lydeen (1993). Southern surface rupture associated with the 1992 M7.4 Landers earthquake: Did it all happen during the mainshock, *Geophys. Res. Lett.* **20**, 2615–2618.

Hutton, L. K., C. E. Johnson, J. C. Pechmann, J. E. Ebel, J. W. Given, D. M. Cole, and P. T. German (1980). Epicentral locations for the Homestead Valley Earthquake Sequence, March 15, 1979, *Calif. Geol.* **33**, 110–114.

Kanamori, H. and D. L. Anderson (1975). Theoretical basis of some empirical relations in seismology, *Bull. Seism. Soc. Am.* **65**, 1073–1095.

Kanamori, H., E. Hauksson, and T. Heaton (1991). TERRAscope and CUBE project at Caltech, *EOS* **72**, 564–565.

Kanamori, H., H.-K. Thio, D. Dreger, E. Hauksson, and T. Heaton (1992). Initial investigation of the Landers, California, earthquake of 28 June 1992 using TERRAscope, *Geophys. Res. Lett.* **22**, 2267–2270.

Klein, F. W. (1985). User's guide to HYPOINVERSE, a program for VAX and PC350 computers to solve for earthquake locations, *U.S. Geol. Surv. Open-File Rept. 85–515*, Menlo Park, California, 24 pp.

Mori, J., J. Filson, E. Cranswick, R. Borcherdt, R. Amirbekian, V. Aharonian, and L. Hachverdian (1994). Measurements of P and S wavefronts from the dense three-dimensional array at Garni, Armenia, *Bull. Seism. Soc. Am.* (in press).

Mori, J. (1994). Rupture directivity and slip distribution of the M4.3 foreshock to the 1992 Joshua Tree earthquake, *Bull. Seism. Soc. Am.* (in press).

Mueller, C. S. (1985). Source pulse enhancement by deconvolution of an empirical Green's function, *Geophys. Res. Lett.* **22**, 33–36.

Ohnaka, M. (1993) Critical size of the nucleation zone of earthquake rupture inferred from immediate foreshock activity, *J. Phys. Earth* **41**, 45–56.

Sibson, R. (1983). Continental fault structure and the shallow earthquake source, *J. Geol. Soc. London* **140**, 741–767.

Sieh, K., L. Jones, E. Hauksson, K. Hudnut, D. Eberhart-Phillips, T. Heaton, S. Hough, H. Kanamori, A. Lilje, S. Lindvall, S. F. McGill, J. Mori, C. Rubin, J. A. Spotila, H.-K. Thio, J. Treiman, B. Wernicke, and J. Zachariasen (1993). Near-field

investigations of the Landers earthquake sequence, April to July 1992, *Science* **260**, 171–176.

Spudich, P. and E. Cranswick (1984). Direct observation of rupture propagation during the 1979 Imperial Valley earthquake using a short baseline accelerometer array, *Bull. Seism. Soc. Am.* **74**, 2083–2114.

Wald, D. J. and T. H. Heaton (1994). Spatial and temporal distribution of slip for the 1992 Landers, California, earthquake, *Bull. Seism. Soc. Am.* **84**, no. 3, 668–691.

Wald, D. J., D. V. Helmberger, and T. H. Heaton (1991). Rupture model of the 1989 Loma Prieta earthquake from the inversion of strong-motion and broadband teleseismic data, *Bull. Seism. Soc. Am.* **81**, 1540–1572.

Wyatt, F., D. C. Agnew, and M. Gladwin (1994). Continuous measurements of crustal deformation for the 1992 Landers earthquake sequence, *Bull. Seism. Soc. Am.* **84**, no. 3, 768–779.

Department of Geological Sciences
University of Southern California
Los Angeles, California 90089-0740
(R.A.)

U.S. Geological Survey
Pasadena, California 91106
(J.M.)

Manuscript received 28 July 1993.